Laboratory Studies of Wind-Driven Langmuir Circulations

ALAN J. FALLER AND ENRIQUE A. CAPONI[1]

Institute for Physical Science and Technology, University of Maryland
College Park, Maryland 20742

Langmuir circulations in a wind wave tank have been observed and measured by a variety of methods including dye patterns and floating surface tracers. On the basis of measurements of cellular wavelength λ_c as a function of surface wavelength λ_w and depth H a tentative functional relation for the dependence of λ_c/H upon λ_w/H is proposed. The experiments clearly imply that the waves play an important role in the mechanism of formation of the Langmuir circulations but that the depth of the layer has a significant modifying influence. On the basis of certain 'rake' experiments and other indirect observations it is proposed that when $\lambda_w/H < 1$, the primary scale of Langmuir circulations, related to λ_w, transfers energy to a larger scale that is commensurate with the depth such that $\lambda_c/H \simeq 2$. Under these circumstances, two distinct scales of Langmuir circulations may exist simultaneously.

INTRODUCTION

Bands and streaks more or less parallel to the wind on natural water surfaces have been recognized and reported for many years. In 1927, Langmuir observed that on the open ocean, floating seaweed lined up in rows parallel to the wind direction with spacings of the order of 100 m, the orientation of the bands changing with the wind. In a remarkable series of experiments on Lake George in New York State he subsequently observed the same phenomenon on a smaller scale, and after several years of occasional observations he concluded [*Langmuir*, 1938], 'The helical vortices set up by the wind apparently constitute the essential mechanism by which the epilimnion is produced.'

There has been little general agreement about the mechanism by which the wind generates the helical rolls and about their relative importance in the oceans. Indeed, it is our experience that many observers or casual readers of the literature seriously doubt that the circulations described by Langmuir do exist in fact. All agree that there is a surface streakiness, but apparently following the philosophy 'out of sight, out of mind,' many ignore the detailed observations of *Woodcock* [1944, 1950], *Sutcliffe et al.* [1963], *Scott et al.* [1969], *Myer* [1971], *Assaf et al.* [1971], and others, as well as those of Langmuir, who have shown that organized cellular circulations extend to a considerable depth. Thus the abundant evidence for the existence of organized rolls cannot be ignored by any serious investigator of the surface mixed layers of lakes and oceans.

In a preliminary paper one of us [*Faller*, 1969] presented the results of some laboratory experiments in which organized longitudinal rolls were clearly observed beneath wind-generated waves. The simplistic dynamical explanation offered at that time, the 'eddy pressure' concept, is clearly incorrect, for it could be interpreted to mean that simple irrotational waves would produce longitudinal rolls having vorticity, in direct contradiction to well-established dynamical principles. Nevertheless, the results and general conclusions of the experimental observations stand. Some of these conclusions were as follows:

1. The crosswind wavelengths of the longitudinal rolls were related to the water depth.
2. The circulations, made evident by dye patterns near the bottom of the tank, extended through the entire depth of water.
3. Thermal convection was definitely ruled out as the major cause of the laboratory circulations.
4. Surface film, when it was present, prevented the generation of both wind waves and longitudinal rolls.

We present here more extensive laboratory observations that demonstrate an apparent effect of the wavelength of the wind waves on the crosswind wavelengths of the rolls in addition to the clear effect of the water depth. Although these experiments cannot unequivocally demonstrate that the laboratory phenomena take place by the same mechanism as that occurring in lakes and oceans, a plot of results from natural situations together with laboratory data suggests that they are essentially the same phenomena. The laboratory data, while suggesting certain interesting aspects of the Langmuir circulations, however, do not clearly identify the mechanism by which these circulations are generated.

The laboratory results should be viewed in relation to the presently viable theories for the generation of Langmuir circulations. Two such theories that are based upon the same essential dynamics but which differ in certain important respects are the models of Craik and Leibovich. The first model (CL 1) [*Craik and Leibovich*, 1976] is based upon the interaction of a crossed-wave pattern (Figure 1) with a shear flow driven by a constant wind stress. According to theory the differential Stokes drift in the crossed-wave pattern (the Stokes drift being a maximum along the traces of the wave crest intersections) twists the vorticity of the wind-driven shear flow into the vorticity of the Langmuir circulations. If this model is followed without reservation, the crosswind wavelength of the longitudinal rolls λ_c would be uniquely determined by $\lambda_c = \lambda_w/(2 \tan \theta)$, where λ_w is the downwind spacing of the wave crest intersections and θ is the half angle of intersection of the two wave trains.

In the more recent model (CL 2) [*Craik*, 1977; *Leibovich*, 1977] the more or less uniform average Stokes drift of a complex wave pattern is believed to act through an instability mechanism that is formally analogous to convective instability by cooling of the free surface. In this case one would expect the initial scale of instability to be related to the wavelength of the waves, through the depth of the layer of the Stokes drift, but as the convection proceeded, one would expect larger convective rolls whose lateral scale would be commensurate with the depth of the fluid layer.

[1] Present address: Systems Group, TRW, Redondo Beach, California 90278.

Paper number 8C0181.
0148-0227/78/078C-0181$01.00

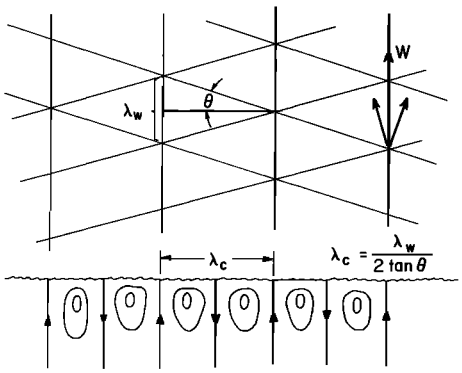

Fig. 1. The pattern of primary Langmuir circulations as they would be related to a pattern of intersecting waves by the CL 1 mechanism. The crests of the two wave trains are represented by the diagonal lines, and ascending motions are beneath the trace of the wave crest intersections. W represents the wind direction and λ_w is defined as illustrated here.

Despite the convincing mathematical arguments of Craik and Leibovich, however, the authors have certain reservations with regard to the importance of these mechanisms. It should be noted that a three-dimensional numerical model by *Mobley* [1976] that was specifically designed to test the CL 1 mechanism failed to give any evidence of the growth of Langmuir circulations under conditions that should have been well suited to their generation. The numerical model correctly predicted the propagation of the intersecting wave patterns and the crosswind variations of the Stokes drift. With the application of a constant wind stress the shear in the water was correctly predicted, but there was no indication of the development of longitudinal rolls as predicted by the analytical theory. Since the numerical model itself is not above criticism, however, one must keep an open mind with respect to these problems. If the CL 1 and CL 2 models are incorrect, it seems likely that the error lies somewhere in the treatment of the upper boundary essentially as a flat surface even though finite amplitude waves are present. For example, in the theory, velocities and vorticities are routinely separated into time averages and fluctuating components, but the definition of a time average near the free surface, where a fixed point sometimes lies above the surface and sometimes below the surface, has not been explicitly considered. It may eventually emerge that when a complex nonlinear interaction of the type envisaged in the CL models is treated, a more exact mathematical treatment of finite amplitude waves will be required. Despite these reservations, however, it must be acknowledged that the CL models at present are the most reasonable candidates for the explanation of the dynamics of the Langmuir circulations.

Principal Experimental Results

The results of our many observations are presented in Figure 2 along with data from certain natural situations. The dependent variate is the wavelength of the cells, λ_c, which corresponds to a pair of counterrotating cells. The parameter λ_c has been made dimensionless by dividing by H, the depth of water for the laboratory observations and the depth of the mixed layer for the oceanic cases.

The abscissa in Figure 2 is the wavelength of the surface waves, λ_w, divided by H. The observations clearly indicate a dependence of λ_c/H upon λ_w/H, and the line

$$\lambda_c/H = 4.8\,[1 - \exp(-0.5\lambda_w/H)] \qquad (1)$$

is our present best estimate of a universal relation for $\lambda_c = \lambda_c(\lambda_w, H)$, if indeed such a relation exists. Thus while the laboratory data probably were not significantly influenced by other variates, it is quite possible that the oceanic data were influenced by such factors as the surface heat flux, internal waves, the strength of the thermocline, etc. The curve of Figure 2 to some extent takes into account suspected systematic errors in the laboratory measurements and in the oceanic observations. In particular, the values of the laboratory measurements of λ_w may be underestimated. Otherwise, for reasons explained below, the line would be drawn through the data of set I.

To plot the oceanic data, we estimated λ_w (in meters) from an empirical relation between wind speed U (in meters per second) and the dominant wavelength in a fully developed sea. This relation was

$$\lambda_w = 2\pi(0.81U)^2/g \qquad (2)$$

which we have adapted from an equation given for wave period by *Neumann and Pierson* [1966, p. 351] and where g = 9.8 m s^{-2}. The use of this formula is quite uncertain, however, because there is no specific knowledge that the sea was fully developed at the time of the various observations, so the estimates of λ_w may be systematically too large for the oceanic data. In addition, for the data of *Faller and Woodcock* [1964] the wind was originally estimated on the Beaufort scale and was later converted to meters per second. Thus the variability of λ_w/H from a smooth curve may be largely explained by these uncertainties.

Nevertheless, the straight line of Figure 2, which passes through the centroid of the solid circles and through the origin, is our best estimate from the oceanic data alone of the possible functional relation that may exist. The CL 1 mechanism, if it is applicable, follows the relation $\lambda_c = \lambda_w/2 \tan \theta$. The straight line of Figure 2 has the slope 1.56 and would correspond to θ = 18°, a value that is not unreasonable. A greater slope would correspond to a lesser angle.

The laboratory data and the field data do not significantly overlap, however, and there are at least two lines of reasoning that may explain this fact. First, the laboratory experiments are restricted by a rigid bottom boundary, while in the ocean,

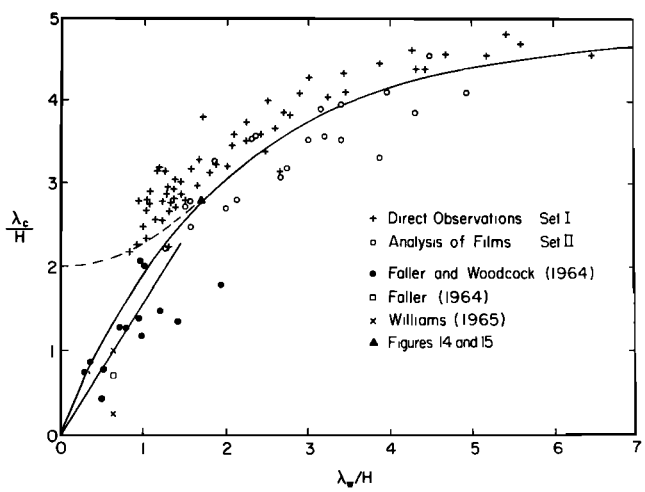

Fig. 2. The dependence of λ_c upon λ_w and H for the laboratory experiments and for the available oceanic data. The solid curve is given by (1). The dashed curve is a possible extrapolation of the laboratory data to account for large secondary circulations at low values of λ_w/H.

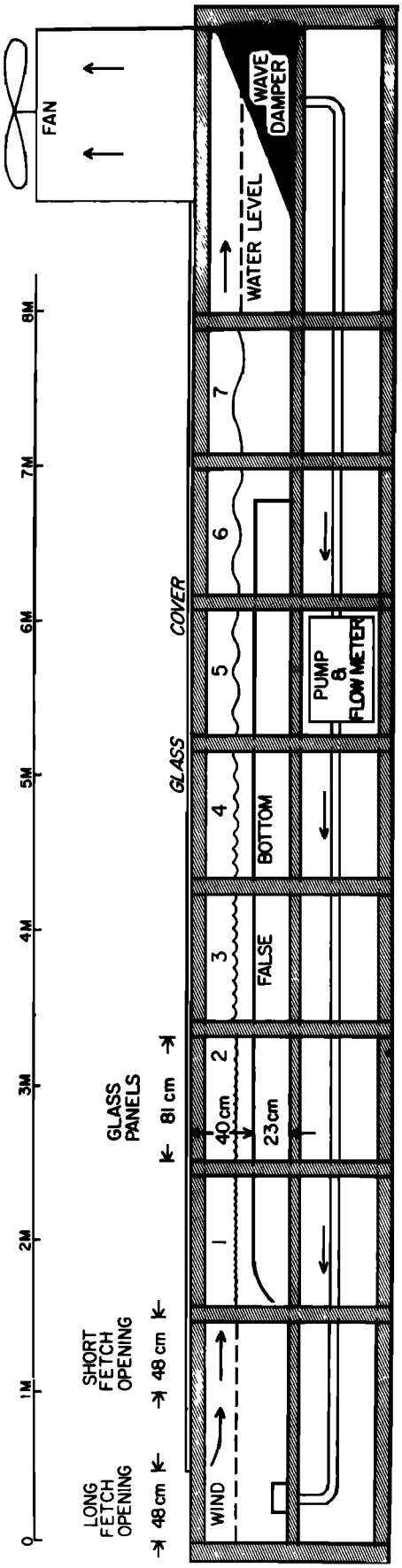

Fig. 3. A diagram of the wind wave tank.

it can be argued, the depth of the mixed layer can be deepened by the strength of the Langmuir circulations. Following this line of reasoning, it is likely that data above $\lambda_c/H = 2$ were not found in the ocean because the Langmuir circulations always tended to increase H according to the strength and scale of the forcing at the surface. For the laboratory limitation of $\lambda_c/H > 2$ it can be argued that lower values simply were not accessible in the experiments.

Second, the oceanic observations were based upon the spacing of convergence lines at the free surface, while the laboratory data were based upon the spacing of convergence lines at the bottom boundary. If there is sometimes a difference in the dominant scales of motion near the surface and near the bottom of the mixed layer, as we suspect, the two sets of data should be considered separately. In particular, we will consider the possibility that in cases where $\lambda_w/H < 1$, there may be a clear separation of a forced primary scale near the surface and a larger secondary scale that occupies the entire mixed layer.

The 'rake experiments,' discussed below, strongly indicate that if small-scale longitudinal rolls are generated in a relatively deep layer of uniform density, significant amounts of energy are transferred to and accumulate in a secondary scale with $\lambda_c/H \simeq 2$. Certain transient experiments and a variety of miscellaneous observations support this conclusion. Moreover, such a transfer of energy to larger scales is favored by the quasi-two-dimensional nature of the longitudinal rolls.

If the data of Figure 2 are viewed in the light of a two-cell model, it may be that the oceanic data represent the scales of the primary mechanism of generation, the depth of the mixed layer being sufficiently deep for the most part that it did not affect the primary scale. Perhaps larger cells existed at the same time, cells that were instrumental in causing the large value of H.

The fact that no laboratory observations were found with $\lambda_c/H < 2.1$ is strongly suggestive that for small λ_w/H the observed λ_c represented secondary depth-limited scales of motion. It would then follow that an extrapolation of the laboratory data to $\lambda_w/H = 0$ should level off and approach the ordinate with zero slope at approximately $\lambda_c/H = 2$. Such a curve could easily be drawn to either set of laboratory data. With such an interpretation it is apparent that it would be inappropriate to draw a single curve to the two sets of data below, say, $\lambda_w/H = 1.5$.

Experimental Apparatus and Procedure

Figure 3 is a diagram of the wind wave tank with the essential dimensions. The primary region of interest is the 5-m-long area over the false bottom where the observations were taken. The width of the tank is $W = 88$ cm, and the water depth H ranged from 2 to 15 cm.

Air was drawn in through an open portion of the tank cover at the left end of the tank by an exhaust fan in the tower at the right end as indicated in the diagram. The fan was controlled by a dc motor and a Variac voltage control with dial settings of $V = 1$–10. Table 1 gives the measured average wind speeds for different Variac settings and two depths of water. These averages were determined visually from the fluctuating needle of a meter connected to a commercial hot wire anemometer and therefore cannot be considered to be accurate to better than ± 10 cm s^{-1}.

The controlled variables in these experiments were the Variac setting V, the fetch F, measured from the downwind edge of the opening in the cover, and the water depth H. The wind speed itself was not directly controlled.

TABLE 1. Average Wind Speeds 5 cm Above the Water Level for Two Values of the Water Depth H and Various Values of the Variac Setting V

	V									
H, cm	1	2	3	4	5	6	7	8	9	10
2.5	17	102	187	251	314	349	398	430	454	488
7.5	35	122	212	288	347	395	432	493	572	623

Units are centimeters per second.

The wavelength λ_w was not measured during each experiment because of the complexity of its determination. Instead, observations of λ_w at various values of F, H, and V were obtained independently of the measurements of λ_c, and as is described in a later section, empirical relations were used for the required values of $\lambda_w(F, H, V)$.

The observations of λ_c were made by using potassium permanganate ($KMnO_4$) dye crystals sprinkled over the white false bottom of the tank. When they were first introduced, these crystals rapidly fell to the bottom and indicated the direction of flow at the bottom by a plume from each crystal. As the crystals dissolved, bands of accumulated dye formed in the regions of horizontal convergence at the bottom as illustrated in Figures 4 and 5. These were also regions of flow upward from the bottom, as could be clearly seen from the motion of the dye. Figure 5 shows a sequence of patterns of crystals and bands in a particularly well formed example.

The dye crystals were distributed over the bottom of the tank in different ways according to the problem at hand. To assume a reasonably uniform distribution of dye across the tank, the crystals were ground out of a pepper grinder onto the glass cover, the grinder being turned continuously as it moved across the cover. The crystals were swept from the cover into the tank through a narrow slot between the plates of the glass cover after temporarily raising the tape that covered the slot. The longitudinal distribution of dye crystals could be controlled by adjusting the wind speed. With no wind the crystals fell in a line across the tank, as in Figures 4 and 5, whereas with a strong wind the crystals were distributed more or less uniformly along the tank over a distance of perhaps 1 m.

In the bulk of our experiments (set I), observations of the number of bands of dye were obtained visually and recorded directly by the observer. At a later time a check was made on the reliability of these visual observations by the recording of the dye patterns on cine' film (set II). But while the filmed data showed the same general trend as the visual data, it was determined later that the films were taken shortly after the start of the wind, a time when the apparent cell spacing was changing significantly, as is explained below.

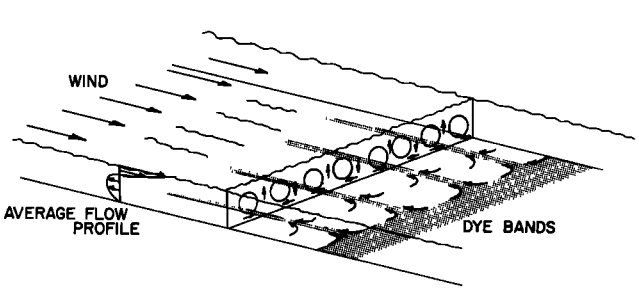

Fig. 4. A schematic diagram of the convergence of dye at the bottom of the wind wave tank due to the action of Langmuir circulations. The bands of dye flow out in a direction counter to that of the wind owing to the return flow at the bottom of the tank.

DETERMINATION OF THE AVERAGE CELL SPACING

By using our dye tracer technique it was always necessary to evaluate crosswind spacing of dye bands in a semisubjective manner, and considerable judgment was involved. Several sources of irregularity and uncertainty, generally associated with transient conditions of one sort or another, could be clearly identified:

1. Shortly after the start of the wind there was a transient period when the average spacing gradually increased (see Figure 6).

2. On several occasions we observed seiching in the tank with periods of 10–15 s, dependent upon the water depth. During periods of longitudinal convergence due to the seiche the vortex structure tended to be destroyed, while during periods of longitudinal divergence the vortex structure was intensified. The latter observation is in agreement with the simple theory of vortex stretching.

3. Under relatively steady conditions the crosswind band spacing frequently was observed to change. This was particularly evident for the larger values of H where there were rather few cells across the tank. One interpretation is that the cell spacing that would have been preferred by the fluid, had it been laterally unrestricted, was incommensurate with the width of the tank. For example, in some early experiments with water 16 cm deep the number of bands was observed to vacillate between 3 and 4 (6–8 cells) with a period of several minutes. In water with a depth of 30 cm the dye patterns indicated a vacillation between 2 and 3 cells with a period of about 20–30 min.

4. Although the apparent longitudinal rolls were generally very long in comparison with their crosswind wavelength, at times variations of the cells along the direction of the wind were clearly present. Some of this variation was certainly associated with the longitudinal growth of λ_w.

For the visual determination of λ_c from an instantaneous observation of bands the following procedure was used. The number of dye bands n_b and the number of clear spaces n_c across the width of the tank W were counted; these correspond to the number of regions of horizontal convergence and horizontal divergence, respectively. The number of cells inferred from the dye pattern was then $N_c = n_b + n_c - 1$. The crosswind average wavelength of the cells for that particular case was then $\lambda_{ci} = 2W/N_c$, there being two cells per wavelength.

Because of uncertainties in counting and because of the natural variability in the number of cells, several determinations of λ_{ci} under identical experimental conditions have been averaged to obtain λ_c and $\sigma_{\lambda c}$, the average and the unbiased estimate of the standard deviation of the individual observation of λ_{ci}. For each data point of set I, from 5 to 15 values of λ_{ci} were obtained under identical conditions of V, H, and F, each value already representing an average across the tank. For our range of values of V, H, and F the values of λ_c ranged

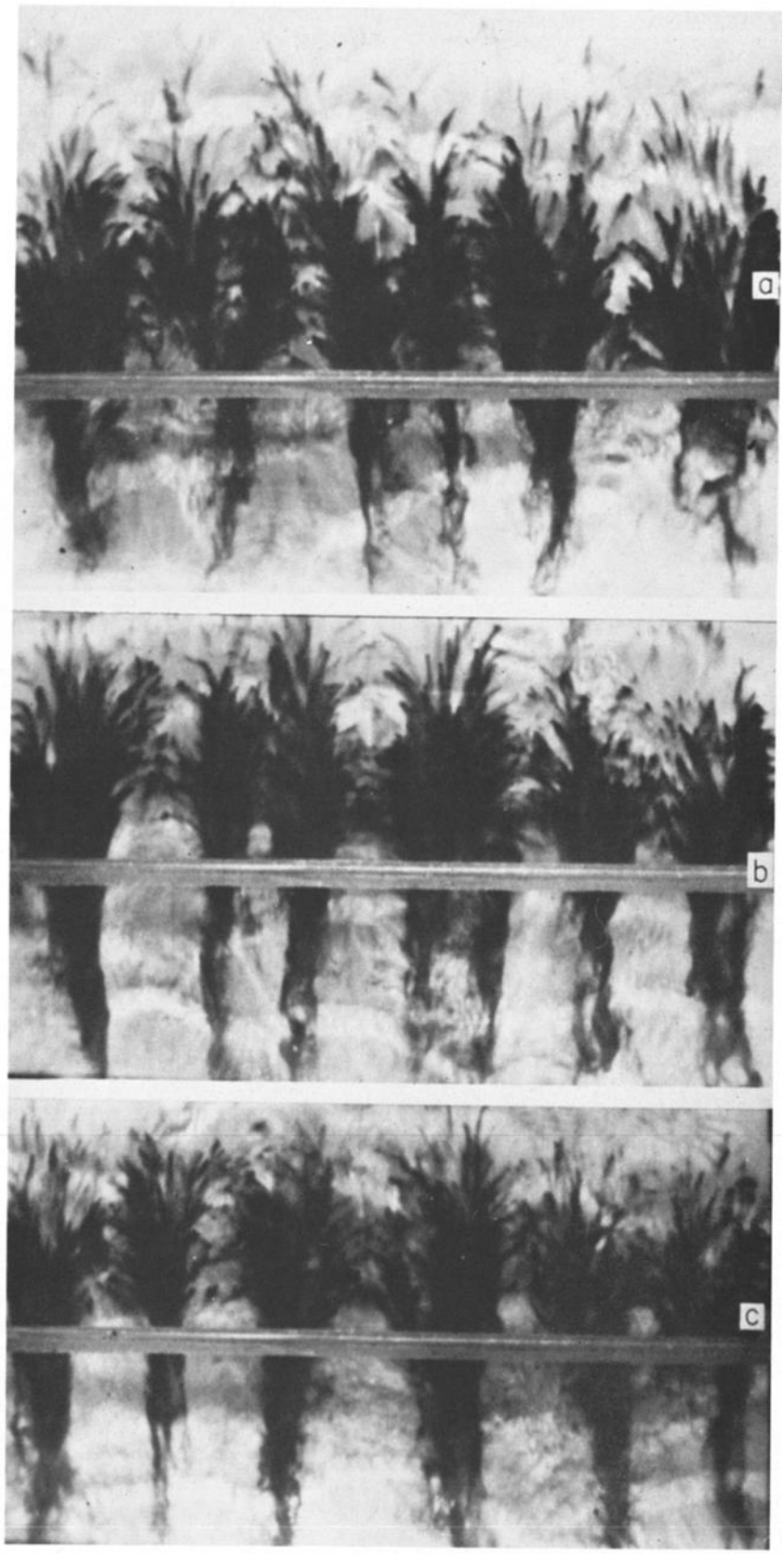

Fig. 5. A sequence of dye patterns illustrating the transient behavior due to time dependence of the Langmuir circulations. (*a*) A pattern found soon after the introduction of dye crystals. (*b*) Taken 4 s after Figure 5*a*. (*c*) Taken 12 s after Figure 5*a*. These photographs were taken in the middle of panel 1 with $V = 8$ and $H = 4$.

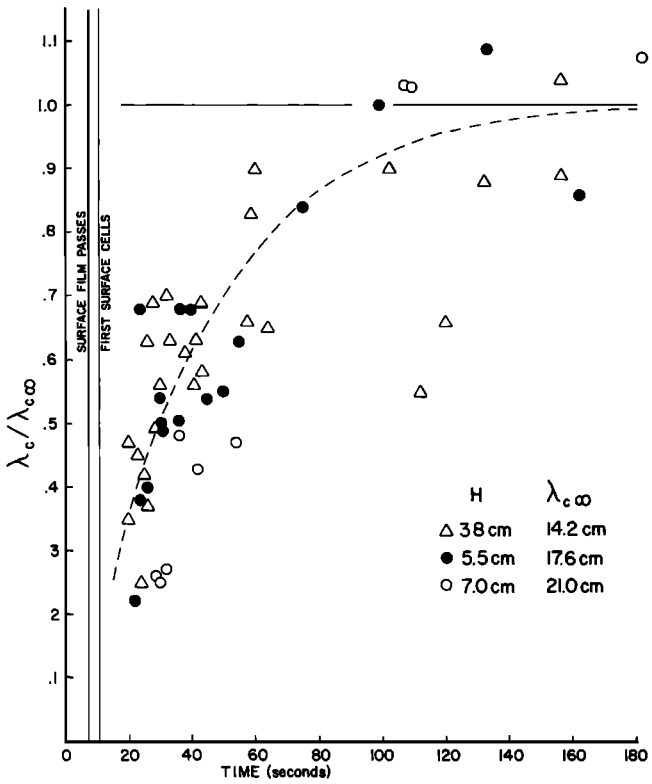

Fig. 6. Time dependence of the apparent cell spacing after turning on the wind. Here λ_c is the stable value of $\lambda_{c\infty}$ that is obtained after a long time. The dashed line is a suggested response curve drawn by eye.

from 5 to 30 cm. The values of $\sigma_{\lambda c}$ were approximately proportional to the values of λ_c, being about 10–15% of λ_c.

Determination of λ_w

The measurement and the description of wind-generated waves present rather serious difficulties even under the relatively well controlled conditions of the laboratory. We sought an estimate of the 'dominant wavelength' λ_w, defined in some objective manner, as a function of V, H, and F.

Figure 7 illustrates a set of three wave patterns as viewed by surface reflections. Attempts to estimate λ_w from such patterns proved to be too subjective, however, and we resorted to the use of wave height profiles along the glass sidewalls of the tank in an attempt to be objective. Various methods were tried, but a major difficulty was that for even a simple crossed wave pattern, as in Figure 1, the location of a longitudinal section (the glass wall) with respect to the pattern is very important and can show quite a few different profiles. In practice, the following procedure was used.

At each of the five glass panels that covered the region of observations of λ_c (see Figure 3) the wave profile was photographed 12 times at intervals of several seconds. This was repeated for different values of V and H. To analyze the wave profiles, the negatives were projected onto the table of a coordinate digital converter, and the coordinates of each crest and trough (subjectively selected) were punched onto paper tape for computer analysis. The spacing between each successive pair of crests and each successive pair of troughs was regarded as determining a single wavelength λ_i. For each such wavelength the wave height (A_i) was determined by the average height of successive wave crests minus the height of the intervening trough or, in the case of successive troughs, by the height of the intervening wave crest minus the average height of the two surrounding troughs. With the set of values of λ_i and A_i (for each set of V, F, and H) a weighted average wavelength was calculated by the formula

$$\lambda_w = \sum_i \lambda_i A_i^2 \Big/ \sum_i A_i^2$$

That is, λ_w was determined by weighting each wavelength by the square of the wave height, an energy-weighted average. This procedure minimized the effect of the many relatively small amplitude shortwaves that were found. Table 2 is an example of the distribution of observed wavelengths and wave heights. While this definition of λ_w is a reasonably objective and consistent one, it may underestimate the value that would be judged to be the dominant wavelength by subjective visual observations by as much as 20%. An example of λ_w is shown in Figure 7*b* for comparison with the wave pattern.

Transient Development of the Cell Spacing

Two independent sets of laboratory data were obtained. The initial experiments, set I, were conducted at the fixed Variac setting $V = 7$. Observations were made at different values of the fetch ranging from $F = 1.27$ m to $F = 4.77$ m. Because F and λ_w were so closely connected in the experiments of set I, a second set of data was taken at fixed F to illustrate unambiguously the effect of $\lambda_w(V, H)$ upon λ_c.

The data of set II were taken at $F = 4.77$ m, and the values of λ_c were analyzed from cine' films of the dye patterns. Upon analysis of the films and reduction of the data it was found that systematic differences existed between the two data sets. Apparently, these differences arose because in each experiment the films were taken shortly after the wind was turned on, whereas the visual observations (set I) were taken several minutes after the start of the wind.

In experiments to determine the time dependence of the cell spacing (Figure 6), the following normal sequence of events occurred:

1. After about 7 s of wind the first waves arrived as the edge of the surface film passed the point of observation.
2. At about 9–12 s, cells were detectable in the surface layer.
3. At about 20 s (this time being quite dependent upon H), dye at the bottom broke up into bands. At this time the ratio $\lambda_c/\lambda_{c_\infty}$ averaged about 0.35.
4. The average value of λ_c gradually increased with time, and after about 2 min the steady state value λ_{c_∞} was attained. This temporal adjustment of λ_c should depend upon the values of V, F, and H, but this dependence has not been explored in detail because of the large uncertainties in any given experiment and the vast number of observations that would be required for definitive results.

The time-dependent results are in reasonable agreement with the differences between the data of sets I and II. Values of λ_c/H for set II are about 0.85 times the values for set I, and from Figure 6 this would correspond to a time of about 1 min after the cells were first observed. This time is in rough agreement with the average time at which the films of set II were taken. It is also apparent from Figure 2 that the data of set II have a slightly larger variance, probably due to the time dependence. Set I thus appears to be the more consistent set of data. The curve of Figure 2 has been drawn somewhat to the right of these data, however, to account for the probable underestimation of λ_w.

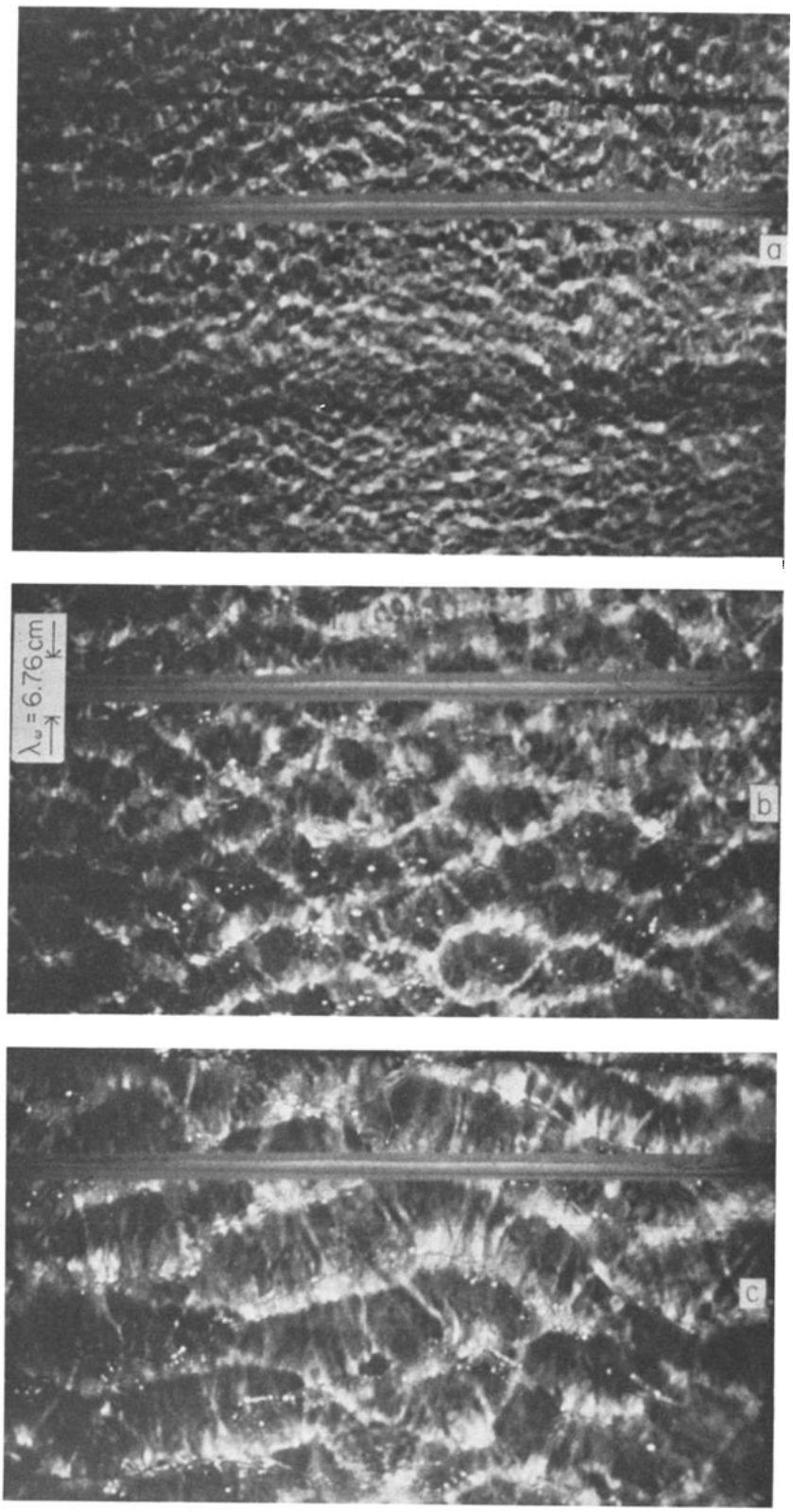

Fig. 7. Examples of wave patterns at panel 1 with H = 10 cm. (*a*) V = 5. (*b*) V = 7. (*c*) V = 9. At the tape (across each photograph), F = 1.48 m. In Figure 7*b* the indicated scale of 6.76 cm is the wavelength λ_w as determined for the conditions of this experiment by empirical relations.

FREE SURFACE FLOATS

Sample trajectories of surface floats are shown in Figures 8*a* and 9*a*. The floats were polyethylene rods 2.54 cm long with 1.27-cm diameter, turned down to about 0.5-cm diameter at the upper end and weighted with a small screw at the lower end so that they would float vertically with only a small section protruding through the surface. The rods therefore averaged the flow in the upper 2.5 cm of water without a significant effect of the wind or of surface tension.

TABLE 2. An Example of the Distribution of Wavelengths Measured From Photographs of the Wave Profile on a Glass Side Panel

λ_w, cm	Number of Cases	Average Amplitude
4–5	3	0.18
5–6	3	0.13
6–7	6	0.24
7–8	12	0.27
8–9	15	0.28
9–10	14	0.36
10–11	31	0.41
11–12	22	0.49
12–13	23	0.55
13–14	15	0.58
14–15	9	0.69
15–16	2	0.50
16–17	5	0.54
17–18	2	0.58
18–19	1	0.58

For each interval of λ_w the number of cases and the average wave height are given. Conditions for this case were H = 10 cm, V = 7, and F = 4.5 m. The energy-weighted average wavelength in this case, from the data summarized above, was λ_w = 12.67 cm.

These tracers can adequately represent the near-surface flow only for scales of motion large in relation to the depth of the floats. If the vertical variation of the horizontal velocity is taken as being proportional to $\cos 2\pi z/K$, where z is depth and K is the vertical wavelength, and if the tracer averages over the depth h, the tracer speed will be proportional to $(\sin Z)/Z$, where $Z = 2\pi h/K$. The ratio of the tracer speed to the free surface speed is then 0.85 for cells 8 cm deep (K = 16 cm) and only 0.47 for cells 4 cm deep. For the experiments represented in Figures 8 and 9 we used h = 8 cm (K = 16 cm).

Approximately 65 floats were lined up across the glass cover next to a taped-over slot. They were inserted by raising the tape and sweeping the row of floats simultaneously through the slot. About 3 s were required for the floats to surface after falling into the water. The motion of the floats was then recorded on 16-mm cine' film at 16 frames per second.

The 7-s trajectories of Figures 8*a* and 9*a* clearly indicate an extension of the tracers into five primary bands with a band at each sidewall. This pattern implies four pairs of cells with an average crosswind wavelength of 22 cm. The banded pattern after 7 s is mainly due to elongation of the tracers along the wind direction, however, and a longer time is required to be certain that the elongations also represent lines of con-

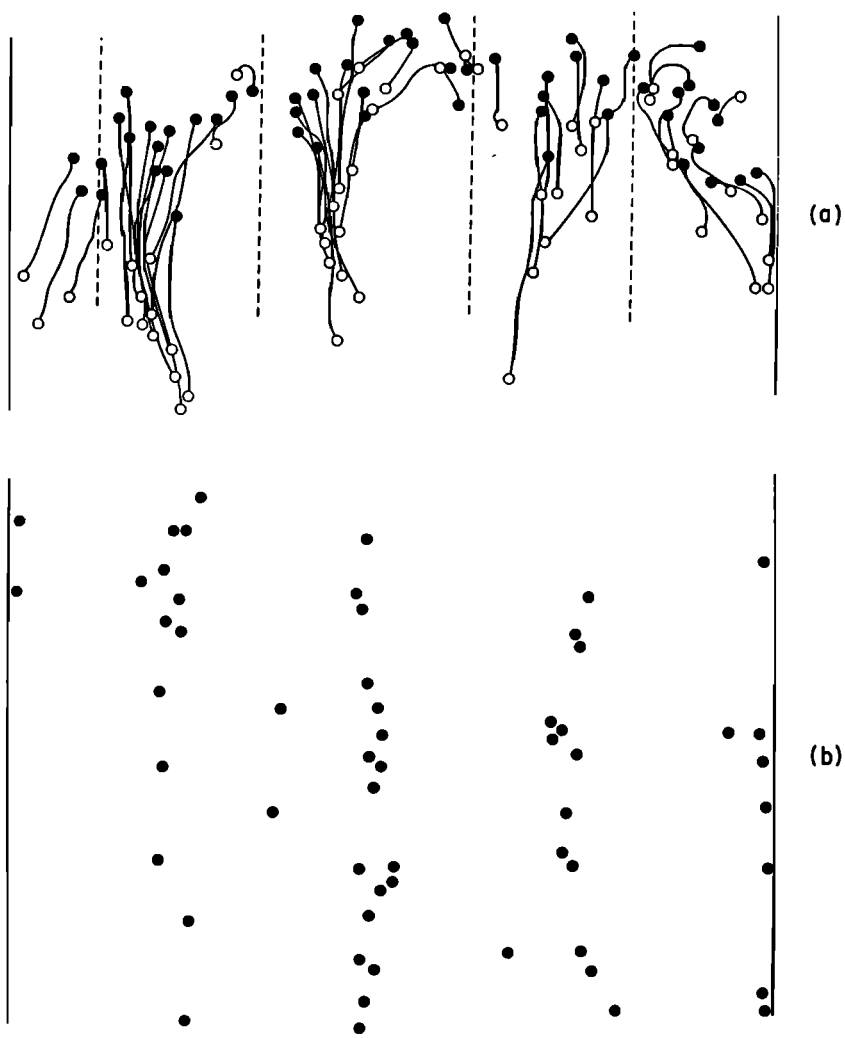

Fig. 8. (*a*) Observed trajectories of surface floats for 7 s under the conditions H = 8 cm, F = 4.77 m, V = 8, and λ_w = 14 cm. Solid circles are the initial positions, and open circles are the positions after 7 s. (*b*) Relative positions of the floats 20 s after the open circles in Figure 8*a*.

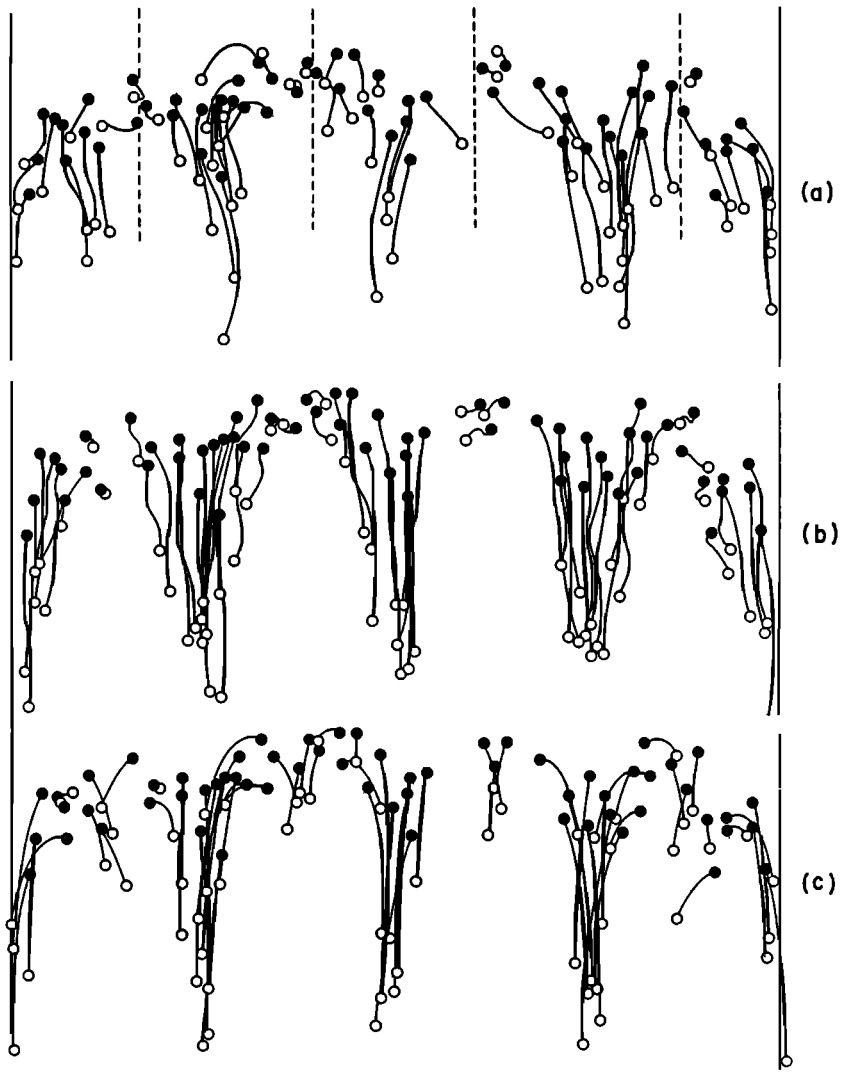

Fig. 9. (*a*) Seven-second trajectories for the same conditions as those in Figure 8*a* but for a different experiment. (*b*) Simulation of the trajectories of Figure 9*a* with single-cell periodic functions for u and v. (*c*) Simulation of the trajectories of Figure 9*a* with two-component periodic functions for u and v.

vergence. Figure 8*b* shows the floats about 20 s after Figure 8*a*, so the convergence into lines is quite clear. The data from these experiments are indicated in Figure 2 by the triangle.

To estimate the speeds of convergence and the along-wind variations of the surface flow, we constructed simple model circulations from which trajectories could be calculated. Figures 9*b* and 9*c* illustrate the results of two such models. In each case the starting positions of the tracers in Figure 9*a* were used, and the cells were assumed to be perfectly regular with L = 22 cm. By taking x and y along and across the tank, respectively, the velocity components for Figure 9*b* were modeled by

$$u = U(1 + \cos 2\pi y/L) + r \tag{3}$$

$$v = -V \sin 2\pi y/L + r \tag{4}$$

where r represents a small random component to simulate wave and turbulence effects. Preliminary estimates indicated that the values of U = 1.6 cm s^{-1} and V = 0.35 cm s^{-1} would be appropriate.

Trajectories were calculated on an HP-25 from the simple difference equations

$$x_{n+1} = x_n + \Delta t U(1 + \cos 2\pi y_n/L) + r_n \tag{5}$$

$$y_{n+1} = y_n + \Delta t V(-\sin 2\pi y_n/L) + r_n \tag{6}$$

with r_n randomly selected in the interval $-0.5 < r_n < 0.5$ cm and Δt = 7/12 s. The trajectories plotted in Figure 9*b* were

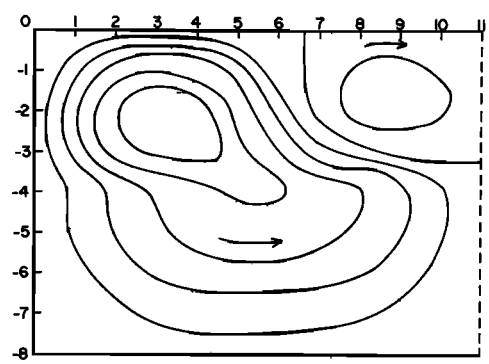

Fig. 10. The stream function corresponding to the simulation used in Figure 9*c*, assuming that the high wave number component occurs only in the upper half of the fluid. Only one of the larger cells is shown.

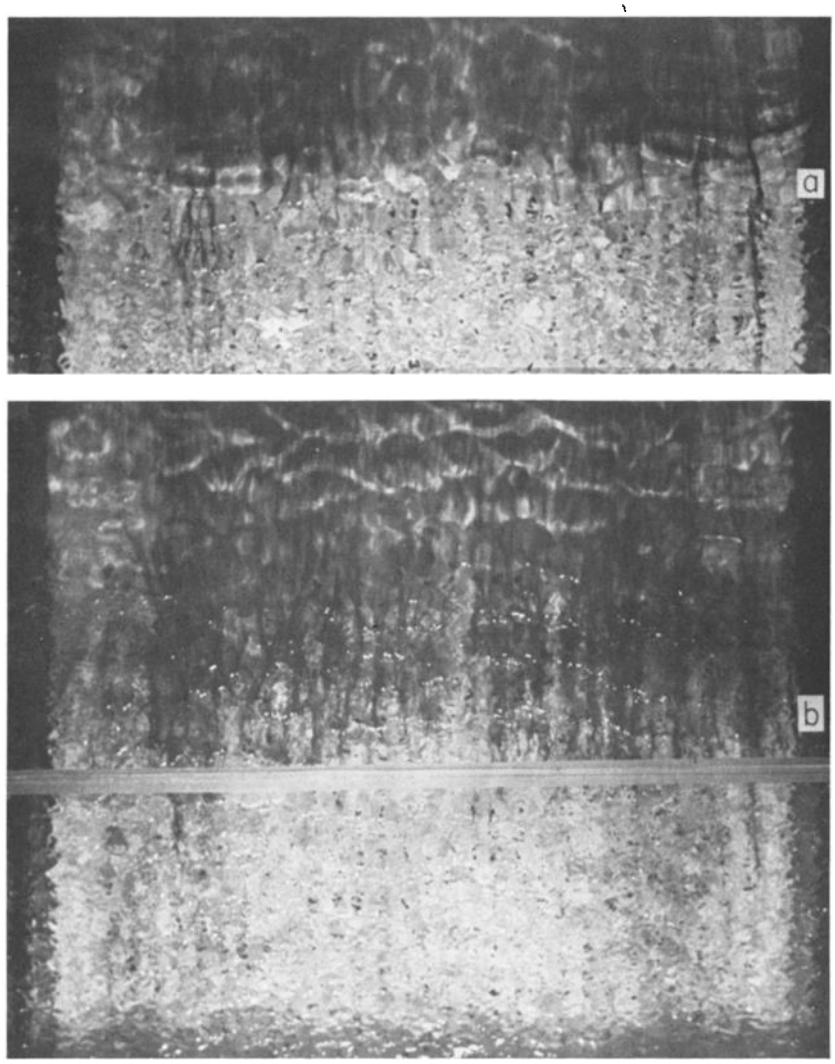

Fig. 11. An example of the breakdown of a laminar surface flow into longitudinal rolls. In Figure 11*a* the flow is primarily laminar, although some streakiness in the dye (moving from top to bottom) can be detected. In Figure 11*b*, 1 s later, the edge of the dye has advanced about 22 cm, and a clear banded pattern is evident with an average band spacing of 2.86 cm.

drawn to the calculated values at every third time step for a total of 12 steps.

Obvious differences exist between the patterns of Figures 9*a* and 9*b*. First, in reality the floats in the convergent regions were not generally advected forward as rapidly as they were in the simulation. This result indicates that the real x component was much more peaked than that of the assumed cosine curve. Second, inspection of the real trajectories between the major convergence lines suggests that there may have been a smaller cellular structure, perhaps with half the wavelength of the large cells. In Figure 8*b*, for example, three floats lie approximately halfway between the major lines.

To correct these deficiencies, we tried the model equations

$$u = U(1 + \cos 2\pi y/L_1 + \cos 2\pi y/L_2) \quad (7)$$

$$v = -V(\sin 2\pi y/L_1 + \sin 2\pi y/L_2) + r \quad (8)$$

a sum of periodic variations with equal amplitudes for each component. The amplitudes and wavelengths were $U = 1.1$ cm s^{-1}, $V = 0.34$ cm s^{-1}, $L_1 = 22$ cm, and $L_2 = 11$ cm. The corresponding trajectories are plotted in Figure 9*c*.

Despite the equal amplitudes of the two cells, the larger cells clearly dominated the convergence pattern, and with the random effects in v all tracers eventually would have converged into the major bands. As was expected, u was more peaked in the second simulation, which was more realistic overall.

The simulation in (7) and (8) was meant to predict the tracer motion, but the tracers averaged the flow over the depth of 2.54 cm. To correct for this averaging effect, let us suppose that the total cellular motion is the linear sum of two components represented by the stream functions

$$\phi_1 = -\Phi_1(\sin 2\pi y/L_1)(\sin \pi z/H) \quad (9)$$

$$\phi_2 = -\Phi_2(\sin 2\pi y/L_2)(\sin 2\pi z/H) \qquad z > -4 \quad (10)$$

where $z = 0$ is at the free surface and z is positive upward. The component ϕ_2 is presumed to act only in the upper half of the fluid, but this does not influence our results other than the pattern in Figure 10. The equations for $v = \partial\phi/\partial z$ and $w = -\partial\phi/\partial y$ are

$$v_1 = -(\pi/H)\Phi_1(\sin 2\pi y/L_1)(\cos \pi z/H) \quad (11)$$

$$v_2 = -(2\pi/H)\Phi_2(\sin 2\pi y/L_2)(\cos 2\pi z/H) \quad (12)$$

$$w_1 = (2\pi/L_1)\Phi_1(\cos 2\pi y/L_1)(\sin \pi z/h) \quad (13)$$

$$w_2 = (2\pi/L_2)\Phi_2(\cos 2\pi y/L_2)(\sin 2\pi z/H) \quad (14)$$

The corresponding amplitudes of v_1 and v_2 are $V_1 = \pi\Phi_1/H$ and $V_2 = 2\pi\Phi_2/H$. For the simulation of Figure 9*c* the amplitudes of the motions of the tracers were assumed to be equal to $V = 0.34$ cm/s for each component. These amplitudes require correction factors, however, so for the 8-cm-deep cell we divide by 0.85, and for the 4-cm-deep cell we divide by 0.47, the values derived earlier in this section. The resultant amplitude estimates are then $V_1 = 0.40$ cm/s and $V_2 = 0.72$ cm/s, and the corresponding stream function and vertical velocity amplitudes are $\Phi_1 = 1.02$ cm^2 s^{-1}, $\Phi_2 = 0.92$ cm^2 s^{-1}, $W_1 = 0.29$ cm s^{-1}, and $W_2 = 0.52$ cm s^{-1}.

The resultant maximum downwelling is calculated to be at $z = -2.23$ cm and is $w_{max} = -0.73$ cm s^{-1}, a value that is in reasonable agreement with visual observations of dye motions. The pattern of flow from the sum of these two simple cells is shown in Figure 10. There it is evident that the larger cell dominates the flow even though the smaller-scale component has larger maximum speeds.

The maximum value of u from (7) is 3.3 cm s^{-1}, but this corresponds to the float motion. The maximum value of the cellularly induced u at $z = 0$ would be considerably larger.

SURFACE DYE PATTERNS

Evidence for banded structure near the free surface by the use of dyes is not so easily obtained because of the strong shear and the turbulence that exist there. There are two situations, however, where we have found it to be possible to obtain clear visual evidence of a well-defined surface structure by using

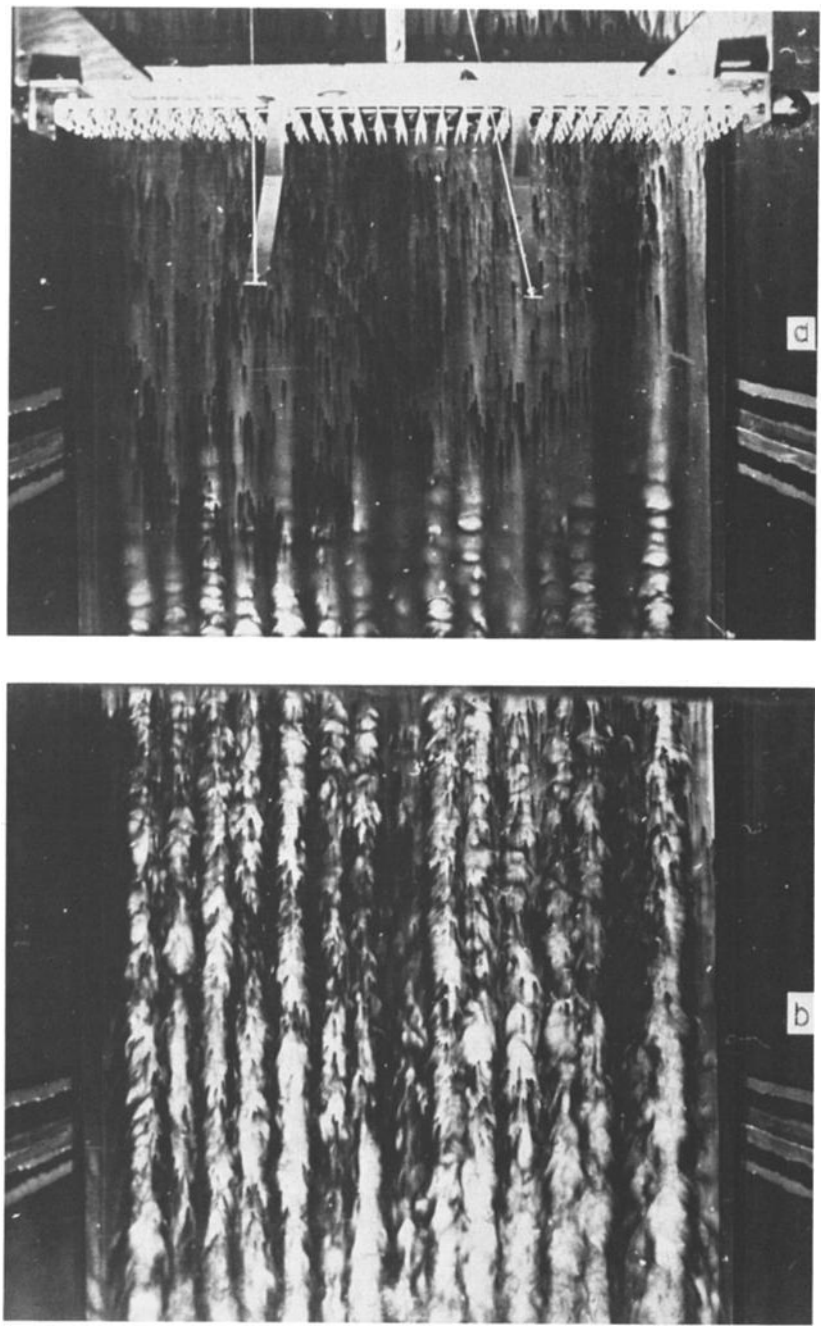

Fig. 12. Cellular patterns produced by pulling the rake through the water at $V_r = 20$ cm s^{-1} and with $H = 2.8$ cm. In Figure 12*a* the moving rake is seen from above, and the rate of formation of patterns at the bottom can be judged by the time delay. The Figure 12*b* photograph was taken 5 s later.

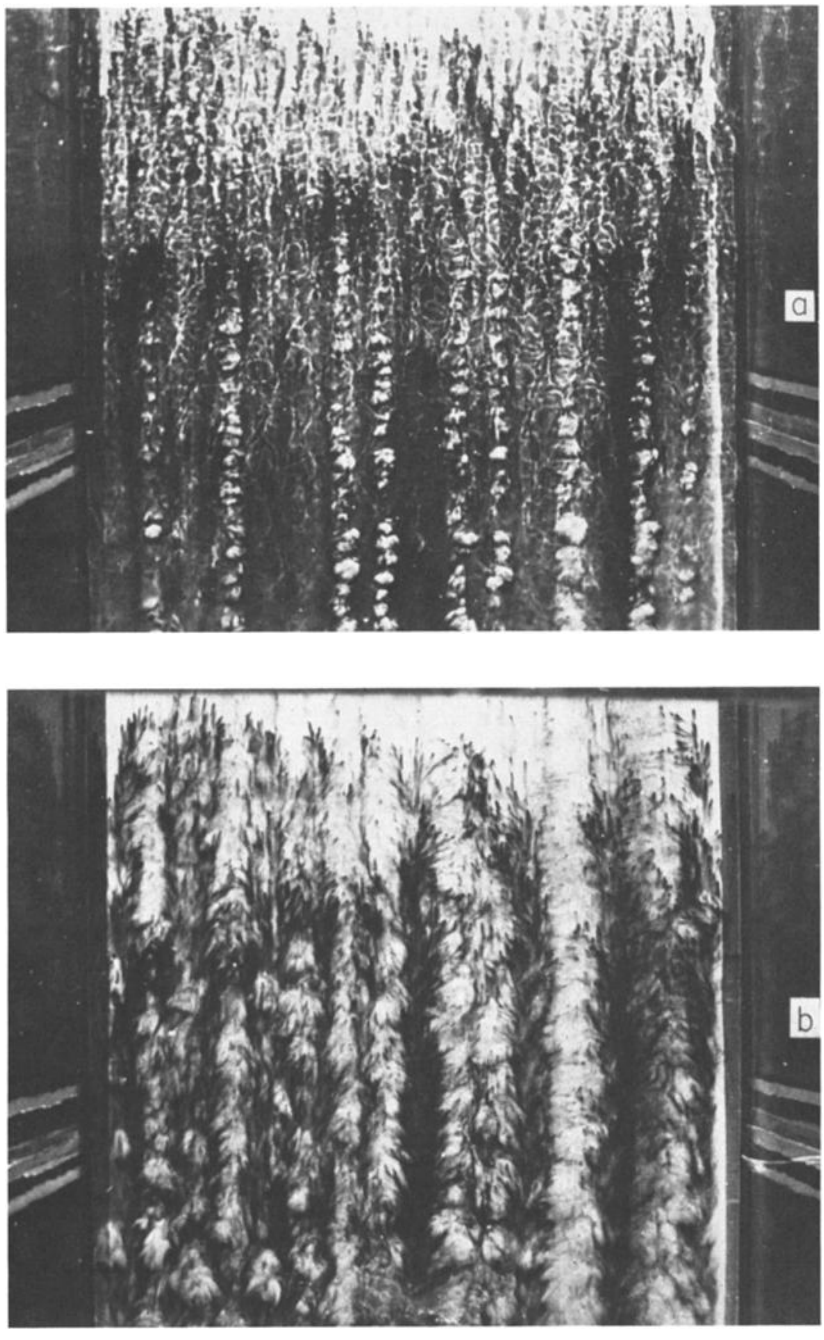

Fig. 13. The same experiment as that in Figure 12 but with $V_r = 100$ cm s^{-1}. The photographs in Figures 13*a* and 13*b* were taken 1 and 5 s after passage of the rake.

dyes. The first situation occurs when very large cellular wavelengths are present, wavelengths large in comparison with scales of turbulence near the surface. The second situation is the transient one when the wind is suddenly applied to a clean water surface. In such a case a careful application of dye powder (methylene blue) or dye crystals (acid fuchsin) to the surface clearly shows the transient occurrence of a banded structure. The dye at first streams out as a more or less uniform sheet of dye, and then, with the advent of a complex wave pattern, it suddenly breaks up into clearly defined bands. The visual evidence for bands lasts but 1 or 2 s because the bands are short lived and because the dye is rapidly diffused.

Figure 11 shows two photographs at the interval of 1 s shortly after the onset of the wind. In Figure 11*a*, streaks of dye may be detected, but there is little in the way of an organized banded structure. In Figure 11*b* a quite regular banded pattern with an average spacing of 2.86 cm may be seen.

At the present time we can make no definite statements about the possible relation of the transient banded structure and the transient wave structure except to say that the presence of a complex wave pattern appears to be necessary for the occurrence of the dye bands. Similar small-banded structures were shown in a cine' film by *McLeish* [1976] at the Second Conference on Ocean-Atmosphere Interactions of the American Meteorological Society, March 30 to April 2, 1976, Seattle, Washington. The following is from McLeish's abstract:

The wind also generated a laminar surface current in the water. The flow underwent a transition to turbulence at a time and fetch that coincided in all cases with the development of the first steep waves. Longitudinal vortices in the water formed as transition intermediates and produced a surface convergence between each pair of wave rows.

RAKE EXPERIMENTS

A number of our experiments have indicated that when small longitudinal rolls are generated in a relatively deep fluid, there is a nonlinear cascade of energy to larger scales. We have supposed that the large cells that will accumulate significant amounts of energy are those that have the approximate ratio $\lambda_c/H \simeq 2$. As an experimental test of this concept we have devised a 'rake experiment' in which small-scale longitudinal rolls are generated in the surface layer by a rake of vanes pulled through the water.

Figure 12*a* is a photograph of the rake from above while it is in use. The series of vanes on each tine of the rake are bent alternately at an angle of $\pm 15°$. Each vane is 1.27 cm high. The tines are spaced at intervals of 2.54 cm across the rake, so with the first two vanes immersed and pulled through the water the rake generates a primary set of longitudinal rolls with $\lambda_{c1} = 5.08$ cm. Of course, turbulence and surface waves also are generated, and slight irregularities in the vanes may directly force larger-scale circulations of small amplitude. In each experiment the rake was pulled through the water at a fixed speed with only two vanes immersed. A small average circulation with a speed of 5.6 cm s^{-1} was forced (by pumping) to provide a means of spreading the $KMnO_4$ dye uniformly over the bottom prior to passage of the rake. For greater depths the flow was proportionately less.

Figure 12 was taken with a water depth $H = 2.8$ cm and with the rake moving at $V_r = 20$ cm s^{-1} opposite to the direction of the relatively slow forced flow, which was maintained during the experiment. The disruption of the dye at the bottom and the obvious formation of bands occurred 2.5 s (50 cm) after passage of the rake, as may be seen in Figure 12*a*. At that time the patchiness of the dye was very similar in appearance to that observed when the turbulence associated with wind-driven circulations reaches the dyed layer at the bottom. Figure 12*b*, 5 s later, shows a well-ordered array of bands, still with the spacing forced by the rake, although not all bands appear to be equally well formed.

Figure 13 shows an experiment identical to that of Figure 12 but with $V_r = 100$ cm s^{-1}, and the photographs were taken 1 and 4 s after passage of the rake. In Figure 13*a* there is abundant evidence that the disturbances from the primary rolls did not all reach the bottom at the same time. This indicates either a slightly unequal rate of generation or an interaction of the smaller scales with larger scales that were also being generated. Figure 13*b* clearly shows larger cells on the right-hand side with spacings about 3 times the primary spacing. This pattern was found to be reproducible and was not due to irregular dye distribution. It must have been related to some small geometrical irregularity of the rake or of the bottom of the tank, but nothing systematic was found.

Figure 14 was for $H = 6.9$ cm and $V_r = 100$ cm s^{-1}. In comparison with Figure 13 the effect of the primary rolls is not at all apparent, and larger scales dominate the circulation. We infer approximately six pairs of cells from this figure, thus obtaining $\lambda_{c2} = 14.6$ cm and $\lambda_{c2}/H = 2.13$.

Noting the apparent importance of small irregularities in the spacings of the tines, we exaggerated this effect by deliberately bending the tines to the right or to the left in a random fashion according to the toss of a coin. Figure 15*a* illustrates the rake after the tines were bent, and Figure 15*b* shows the pattern of flow at the bottom that was generated in 13.9 cm of water with $V_r = 100$ cm/s. There appears to be two major regions of convergence, but there is also convergence at each wall. If we infer three pairs of cells, we obtain $\lambda_{c2} = 29.3$ cm and $\lambda_{c2}/H = 2.1$, although this estimate is somewhat uncertain. Inspection of the pattern of tines in Figure 15*a* gives no particular evidence that the pattern of the cells was directly caused by the pattern of the tines.

Figure 16 illustrates the application of the same irregular rake to a water depth of 9.5 cm. In this case the bottom two

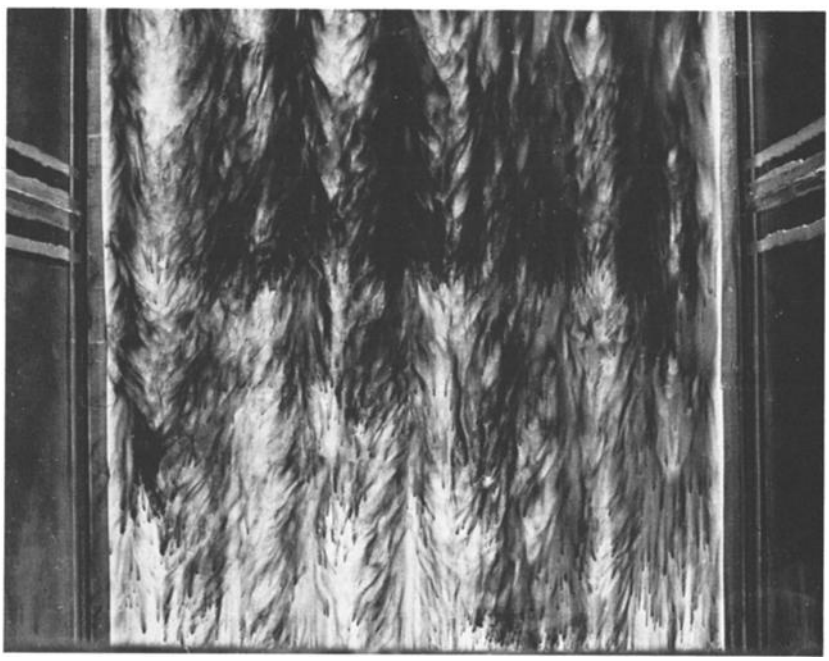

Fig. 14. The rake experiment with $H = 6.9$ cm and $V_r = 100$ cm s^{-1}.

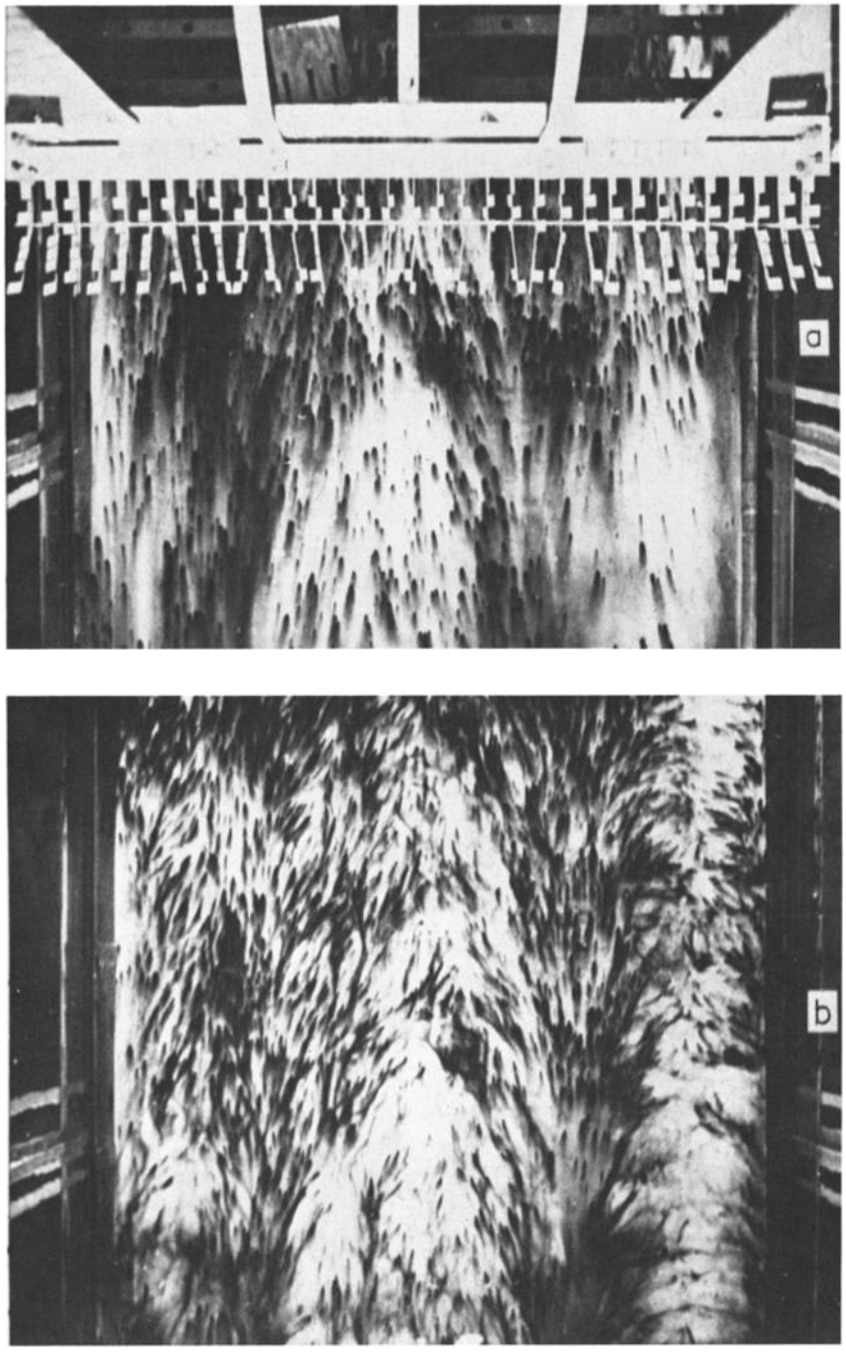

Fig. 15. (*a*) The rake after randomly bending the tines right or left according to the toss of a coin. (The dye pattern in Figure 15*a* is left over from a previous trial.) (*b*) The pattern of flow generated by the irregular rake for H = 13.6 cm and V_r = 100 cm s^{-1}.

vanes were immersed to the depth interval 2.5–5 cm, and the upper vanes were straightened. In Figure 16*a* the scale of the initial patchiness at the bottom was clearly larger than that shown by Figures 12 and 13 and had an average wavelength of 6.7 cm, $\lambda_c/H = 0.71$. Figure 16*b*, however, taken a few seconds later, seems to show about five pairs of cells with the corresponding ratio λ_{c2}/H = 1.85 cm.

These few examples of the rake experiments clearly show the cascade of energy to larger scales and they seem to indicate that after some time the dominant scale will have a ratio $\lambda_c/H \simeq 2$. Improved experiments with a better mechanism for the generation of the surface cells and with better observational techniques would be necessary to be more definitive. Computer experiments with two-dimensional rolls would be helpful but might not effectively simulate the effects of turbulence.

DISCUSSION

Natural conditions have not been precisely modeled in these experiments because of laboratory limitations. Nevertheless, we believe that many of the fundamental features of the Langmuir circulations are exhibited in these results. Natural conditions most like those of the laboratory may be found in shallow lakes or mud flats where the bottom boundary is an important factor. These are also the conditions under which the most regular Langmuir circulations are observed.

With an ideal state of steady and horizontally uniform con-

ditions, and with a fixed depth and well-mixed fluid, the most significant nondimensional parameter to describe the flow should be a Reynolds number given by

$$Re = u_* H/\nu$$

where u_* is the friction velocity in the air (square root of the surface wind stress per unit mass), for the waves, the shear flow, and the turbulence, and hence the Langmuir circulations, should all depend primarily upon u_*, H, and ν. For a comparison of Re in the laboratory and in natural conditions we have made a crude estimate of u_* for a typical laboratory experiment. From Table 1 the basic values are, for $H = 7.5$ cm and $V = 7$, wind speed $U = 432$ cm s^{-1} at $z = 5$ cm above the water surface. Using *Charnock*'s [1950] relation

$$z_0 = u_*^2/81.1g$$

and the logarithmic profile

$$U = u_* k^{-1} \ln z/z_0$$

where z_0 is the roughness length and $k = 0.4$, we find $u_* = 27.5$ cm s^{-1} and $Re = 20{,}600$. The applicability of Charnock's relation to the laboratory experiment is highly questionable because of the lack of a fully developed air flow and fully developed waves and because of the constraints of the bounda-

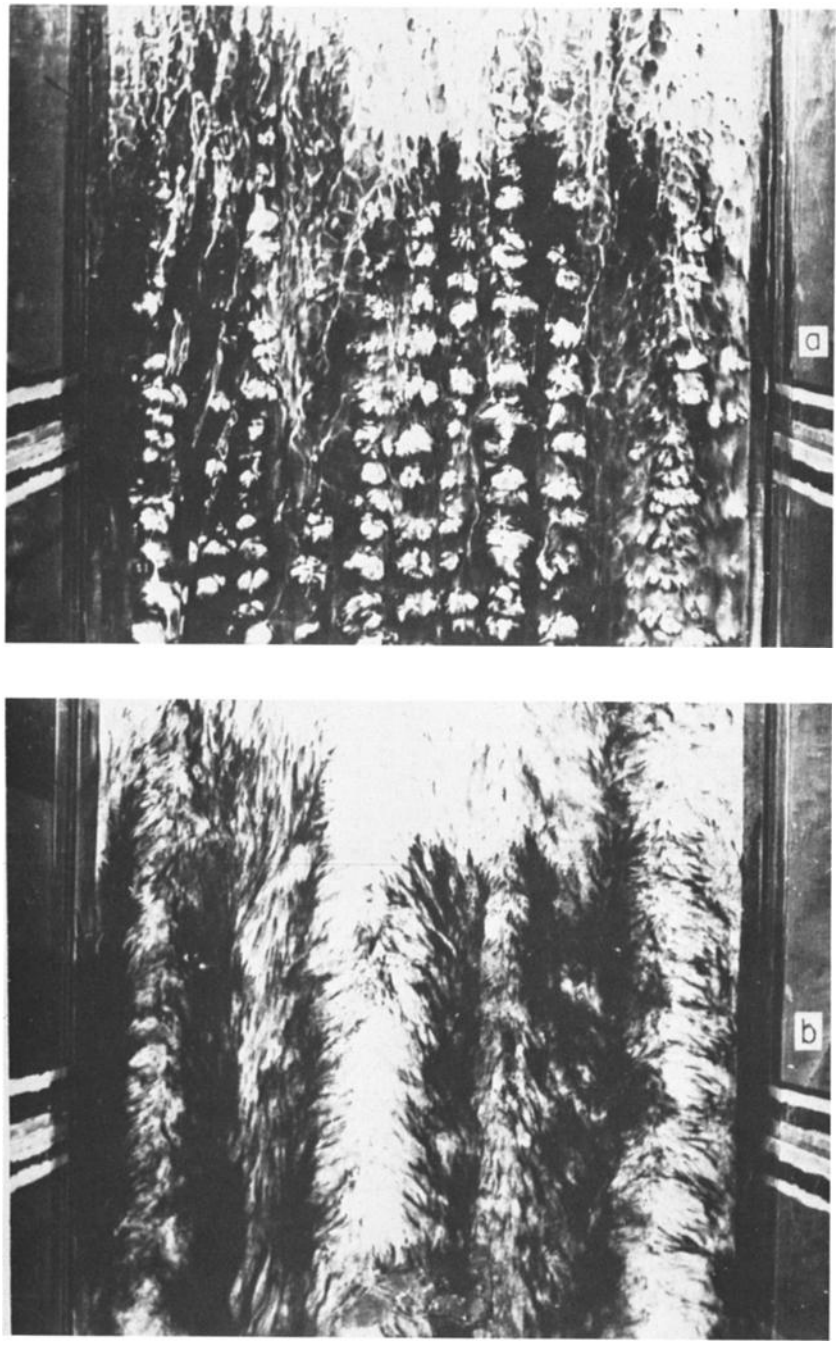

Fig. 16. An experiment with the irregular rake for $H = 9.5$ cm and $V_r = 100$ cm s^{-1}. (*a*) The initial turbulence pattern shortly after passage of the rake. (*b*) The flow pattern several seconds later.

ries on the air turbulence and on the waves. Nevertheless, this result is not particularly sensitive to the value of z_0 because of the logarithmic dependence.

Over natural water surfaces the same value of u_* occurs for a wind speed of about 5 m s^{-1} (at z = 10 m), so that the largest variations in Re are probably due to the variation of H. As a rule the laboratory circulations were most well developed at the higher wind speeds and at the greater depths, i.e., larger values of Re. Therefore we are confident that the Langmuir circulations in shallow lakes, which occur with only slightly larger values of Re, are essentially the same phenomenon as that in the laboratory experiments.

Some experiments were conducted with forced flow (by pumping) both with and against the wind. No obvious differences were observed in the scales of the Langmuir circulations except that with a strong longitudinal flow at the bottom it was more difficult to discern the pattern of cross flow clearly. Accordingly, most experiments were carried out with no pumping, so that only the return flow at the bottom and the downward advection of momentum caused longitudinal streaming from the dye crystals.

A variety of shear profiles with and without return flow should be expected in shallow lakes and in tidal flats, but in view of the CL theories it is likely that the shear flow near the surface, rather than the mean flow or the shear near the bottom, should be the important parameter in this problem. If an independent shear flow (other than that driven by the wind) is important, it should probably be entered into the problem in the form of a nondimensional number of the form

$$Re_2 = (\nu \partial u/\partial z)^{1/2} H/\nu$$

and experiments should be devised to test this question. The Langmuir number used by *Leibovich* [1977] is appropriate for conditions (theoretical models, laboratory experiments) where the waves, the shear flow, and the turbulence are independently specified. Of course in the presence of stratification or if the earth's rotation is a significant modifying influence, other nondimensional numbers enter the problem.

Shallow water cases have been reported by *van Straaten* [1950] for water from 1 cm to a few meters deep. He found that the ratio of streak spacings to depth fell in the range 2–4, but no more precise relation between the depth and the spacing was obvious. He also quoted observations by Seilkoff (communicated by *Neumann* [1948]) in the Baltic near the German coast where spacings of 8–10 m in a water depth of 2 m were found. Presumably, in these shallow water cases where the ratio λ_c/H ranged from 2 to 5, there were large ratios of λ_w/H.

Observations of λ_c in the ocean generally have not been accompanied by observations of both λ_w and H, and most of the oceanic observations in Figure 2 have used the empirical relation in (2) to obtain λ_w. Therefore our analysis of the oceanic data and the curves that have been drawn in Figure 2 must be considered speculative. There are, however, several references in the literature to the simultaneous observation of more than one scale of Langmuir circulation in deep water. The observations by *Williams* [1965], which are plotted in Figure 2, are of one of the best documented cases. *Assaf et al.* [1971] found evidence for three simultaneous scales of approximately 200, 50, and 5 m from patterns of dye and found that in the presence of large Langmuir circulations the Ekman boundary layer showed no spiral characteristics. On another occasion, however, when only small-scale Langmuir circulations were present ($\lambda_c \simeq 5$ m), the Ekman spiral was well developed.

CONCLUSIONS

The laboratory experiments have clearly demonstrated an important effect of λ_w upon λ_c. These results therefore tend to confirm theories in which the scale of the waves plays an important role in the mechanism and scale of the Langmuir circulations. But the experiments cannot distinguish between the CL 1 and the CL 2 mechanisms nor between these and any other mechanisms that may involve the waves.

The simple kinematic and ad hoc cellular model provided in the section on surface floats is instructive in several ways. First, by comparison with the observed surface trajectories it (1) provides estimates of the convergent speeds at the surface and corrections for the depth integrations of the floats, (2) clearly illustrates the concentrated nature of the longitudinal surface jets, a conclusion that could not be justified by inspection of the trajectories alone, without comparison with a model, and (3) suggests that more than one identifiable scale of circulation was present at the surface. The appearance of more than one organized scale of motion is an important departure from the numerically calculated single-cell model of *Leibovich and Radhakrishnan* [1977], which, because it was a fully nonlinear calculation, also produced a concentrated downwelling and a concentrated surface jet. Second, the simple linear superposition of two cellular structures illustrates (1) the dominance of the larger scale upon the pattern of streamlines and the motion of Lagrangian tracers and (2) the complex pattern of vertical velocities that may be expected (as in Figure 10) when one departs from the single-cell concept.

The rake experiments, although not conclusive in themselves, strongly support our supposition that in deep water, directly forced small scales of circulation will transfer significant energy to larger scales. Apparently, the dominant scale that will eventually emerge will have the ratio $\lambda_c/H \approx 2$, although further controlled experiments of this type or fully three-dimensional numerical calculations should be carried out.

The significance of these results is that under certain conditions we may well expect more than one scale of motion to contain significant energy, that the larger scale will probably be more evident from Lagrangian tracers and may dominate the vertical exchange of heat and momentum, and that the more obvious scale may not represent the primary driving mechanism.

Acknowledgments. The research reported here has been supported in part by the National Science Foundation under grants NSF GA 26026, DES-74-24132A01, and ATM 76-82061. Publication 77-170 of the Meteorology Program, University of Maryland, College Park.

REFERENCES

Assaf, G., R. Gerard, and A. L. Gordon, Some mechanism of oceanic mixing revealed in photographs, *J. Geophys. Res., 76,* 6550–6572, 1971.

Charnock, H., Wind stress on a water surface, *Quart. J. Roy. Meteorol. Soc., 81,* 639–640, 1950.

Craik, A. D. D., The generation of Langmuir circulations by an instability mechanism, *J. Fluid Mech., 81,* 209–223, 1977.

Craik, A. D. D., and S. Leibovich, A rational model of Langmuir circulations, *J. Fluid Mech., 73,* 401–426, 1976.

Faller, A. J., The angle of windrows in the ocean, *Tellus, 16,* 363–370, 1964.

Faller, A. J., The generation of Langmuir circulation by the eddy pressure of surface waves, *Limnol. Oceanogr., 14,* 504–513, 1969.

Faller, A. J., and A. H. Woodcock, The spacing of windrows of *Sargassum, J. Mar. Res., 22,* 22–29, 1964.

Langmuir, I., Surface water motion induced by wind, *Science, 87,* 119–123, 1938.

Leibovich, S., Convective instability of stably stratified water in the ocean, *J. Fluid Mech., 82,* 561–581, 1977.

Leibovich, S., and K. Radhakrishnan, On the evolution of the system of wind drift currents and Langmuir circulations in the ocean, *J. Fluid Mech., 80,* 481–507, 1977.

McLeish, W., Wave growth during a laminar-turbulent transition in water (abstract), *Bull. Amer. Meteorol. Soc., 57,* 141, 1976.

Mobley, C., A numerical model of wind and wave generated Langmuir circulations, Ph.D. dissertation, Meteorol. Program, Univ. of Md., College Park, 1976.

Myer, G. E., Structure and mechanism of Langmuir circulation on a small inland lake, Ph.D. dissertation, State Univ. of N. Y., Albany, 1971.

Neumann, G., Bemerkungen zur Zellularkonvektion im Meer und in der Atmosphäre, *Ann. Meteorol., 1,* 235–244, 1948.

Neumann, G., and W. J. Pierson, Jr., *Principles of Physical Oceanography,* 545 pp., Prentice-Hall, Englewood Cliffs, N. J., 1966.

Scott, J. T., G. E. Myer, R. Stewart, and E. G. Walther, On the mechanism of Langmuir circulations and their role in epilimnion mixing, *Limnol. Oceanogr., 14,* 493–503, 1969.

Sutcliffe, W. H., E. R. Bayler, and D. W. Menzel, Sea surface chemistry and Langmuir circulation, *Deep Sea Res., 10,* 233–243, 1963.

van Straaten, L. M. J. U., Periodic patterns of rippled and smooth areas on water surfaces, induced by wind action, *Proc. Neth. Acad. Sci., 53,* 2–12, 1950.

Williams, K. G., Turbulent water flow patterns resulting from wind stress on the ocean, *Mem. Rep. 1653,* U.S. Naval Res. Lab., Washington, D. C., 1965.

Woodcock, A. H., A theory of surface water motion deduced from the wind-induced motion of the Physalia, *J. Mar. Res., 5,* 196–205, 1944.

Woodcock, A. H., Subsurface pelagic sargassum, *J. Mar. Res., 9,* 77–92, 1950.

(Received November 15, 1977;
revised February 14, 1978;
accepted February 16, 1978.)